Design of Programmable Gaussian-Derived Wavelet Filter for Wearable Biomedical Sensor

Yuzhen Zhang, Wenshan Zhao and Yichuang Sun

Abstract—To provide multiple options for specific application in bio-signal processing, the programmable Gaussian-derived Gm-C wavelet filter has been proposed. To realize the programmable characteristic, the analog wavelet base with one numerator term is constructed by using hybrid artificial fish swarm algorithm. Also, the inverse follow-the-leader feedback Gm-C filter structure with a switch array is employed. By programming switches only, Gaussian and Marr wavelet transforms can be realized flexibly with all component parameters unchanged. The seventh-order programmable wavelet filter is designed as an example. Simulation results show that power consumption is only 141.68 pW at scale a=0.1, with dynamic range of 42.6 dB and figure-of-merit of 2.05×10^{-13}. Due to the programmability, the proposed design method can implement two wavelet filters with very low circuit complexity.

KEYWORDS—Wearable biomedical sensor, Physiological signal processing, Gaussian-derived wavelet transform, Programmability, Hybrid artificial fish swarm algorithm, Analog filter.

I. INTRODUCTION

Owing to the high-order vanishing moment, Gaussian-derived wavelets have been widely applied in various areas. Especially, as the first and second derivative of Gaussian function, Gaussian and Marr wavelets are extensively used in feature extraction of physiological signals, e.g., electroencephalogram (EEG) and electrocardiogram (ECG) [1]-[8]. Along with the emergence of intelligent medical device, wearable biomedical sensor integrated with wavelet transform for on-line feature extraction has attracted much attention. In this context, the analog implementation of Gaussian and Marr wavelet transforms has been investigated due to low power compared with digital counterpart, but limited to generate fixed-type wavelet base [1]-[4]. So far, the selection of wavelet base is still a major concern since the best wavelet base can be varied depending on specific biomedical signals [9]-[11]. Furthermore, multimodal measurement of physiological signals has been considered as a promising technique in healthcare monitoring and management. For example, multimodal analysis of EEG and ECG has been employed to improve the seizure detection performance [12]-[15].

Consequently, it is indeed necessary to design a programmable wavelet filter for wearable biomedical sensor, which can flexibly provide multiple Gaussian-derived wavelet bases ready for being selected for specific bio-signal processing as shown in Fig. 1. To date, several design methods for analog wavelet filter have been proposed, nonetheless, they only realize fixed-type wavelet transform. Theoretically, multiple Gaussian-derived wavelet transforms can be realized directly by combining fixed-type wavelet filters. However, to enhance approximation accuracy, high-order wavelet filters with complex poles and zeros are normally used. Thus, this design strategy will inevitably lead to high circuit complexity that is undesirable in wearable application where power and size budgets are both very stringent.

To alleviate aforementioned difficulty, this paper aims to propose a programmable wavelet filter capable of realizing multiple Gaussian-derived wavelet transforms with low power consumption and small chip size. To achieve this goal, the Gaussian-derived wavelet base is approximated by the rational function with only one term in numerator. The approximation is conducted in time domain, in which a mathematical approximation model is constructed and the hybrid artificial fish swarm algorithm (HAFSA) is employed to find the optimal solution. Also, the Gm-C filter structure based on inverse follow-the-leader feedback (IFLF) configuration is used to synthesize the obtained approximation function. Simulation results show that the programmable wavelet filter can realize Gaussian and Marr wavelet transforms flexibly by using minimum component. Using SMIC 1V 0.18μm CMOS technology, the power consumption of designed programmable wavelet filter at scale a= 0.1 is only 141.68pW.

This work was supported in part by the National Natural Science Foundation of China under Grant 61504008, in part by the Fundamental Research Funds for the Central Universities under Grant 2018JBM005.

Yuzhen Zhang and Wenshan Zhao are with School of Electronic and Information Engineering, Beijing Jiaotong University, Beijing 100044, China (e-mail: wshzhao@bjtu.edu.cn).

Yichuang Sun is with School of Engineering and Technology, University of Hertfordshire, Hatfield AL10 9AB, U.K.

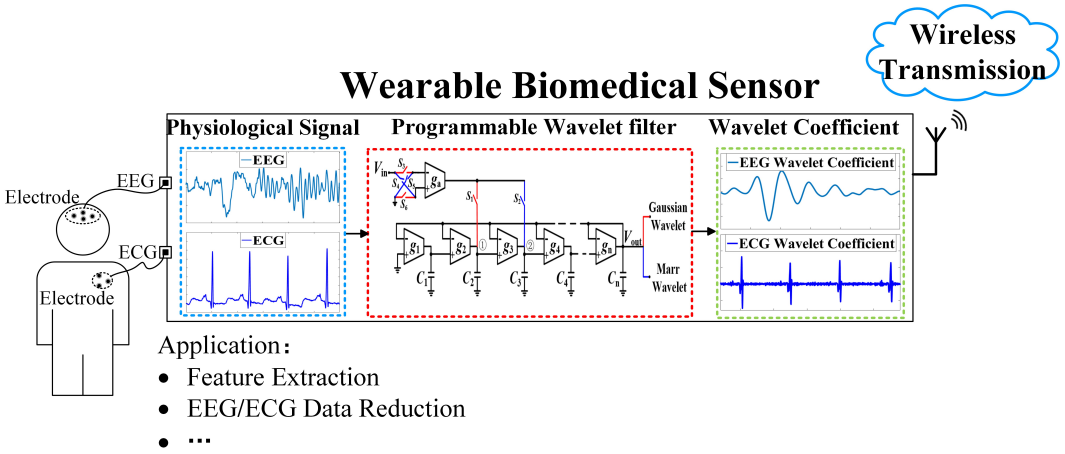

Figure 1. Wearable biomedical sensor integrated with programmable wavelet filter.

Design Strategy for Programmable Gaussian-Derived Wavelet Filter

Continuous wavelet transform (CWT) can be expressed as the convolution of input signal $f(t)$ with wavelet base $\psi(t)$ [3], i.e.,

$$WT_a = f(t) \otimes \frac{1}{\sqrt{a}} \psi(\frac{-t}{a}) \tag{1}$$

where a is the scale parameter.

Apparently, the CWT at scale a can be realized by wavelet filter whose impulse response is $(1/\sqrt{a})\psi(-t/a)$. Therefore, analog implementation of wavelet filter mainly includes the rational approximation of wavelet base (i.e., analog wavelet base) and the synthesis by analog filter structure [3].

Gaussian-derived wavelet bases are constructed by the derivative of Gaussian function and have the general form as

$$\psi_a(t) = \frac{\mathrm{d}^m}{\mathrm{d}t^m}(\frac{1}{\sqrt{a}} e^{-\frac{(t/a)^2}{2}}) \tag{2}$$

Herein, two commonly used wavelets, i.e., Gaussian and Marr wavelets, are considered, which can be obtained by setting m=1 and m=2 (added by a minus sign) in (2), respectively.

In addition, the Laplace Transform of derivatives can be deduced as

$$L\{f^{(n)}(t)\} = s^n L\{f(t)\} \tag{3}$$

Based on (2) and (3), it can be concluded that the rational approximation of Marr wavelet in frequency domain can be obtained easily by multiplying that of Gaussian wavelet by s with a minus sign added. Inspired by above characteristic, the design strategy for programmable Gaussian-derived wavelet filter is discussed as below.

First, the rational approximation to Gaussian wavelet should have minimum terms in numerator. Otherwise, the approximation to Marr wavelet obtained based on (3) may be improper rational expression and cannot be synthesized by analog filter. Meanwhile, keeping numerator terms minimum can facilitate lowering circuit complexity since two Gaussian-derived wavelet filters can share a great part of implementation circuits. Among all the approximation methods, the approach proposed in [3] has the unique advantage in programmable wavelet filter design, since the obtained analog wavelet base only has one numerator term. For example, the general form for analog Marr wavelet base is given as

$$H_{\mathrm{M}}(s) = \frac{-As^2}{B_n s^n + B_{n-1} s^{n-1} + B_{n-2} s^{n-2} + \cdots + B_1 s + 1} \tag{4}$$

Based on (3), the analog Gaussian wavelet base can be deduced as

$$H_{\mathrm{G}}(s) = \frac{As}{B_n s^n + B_{n-1} s^{n-1} + B_{n-2} s^{n-2} + \cdots + B_1 s + 1} \tag{5}$$

Second, to achieve the goal of programmability, filter structure for synthesizing denominator and numerator of analog wavelet base should be independently controllable. In this paper, the Gm-C filter structure based on IFLF configuration is employed [4],[16]. Compared with other structures, IFLF filter structure fully meets above requirement, based on which the circuits for synthesizing the denominator of (4) and (5) can be shared. More importantly, IFLF structure only requires one Gm cell to realize the only numerator term, which provides the possibility of programmable realization. Also, Gm-C technique is well suited for low-power and multi-scale wavelet filter design since transconductor has the characteristics of open loop operation, circuit simplicity and tunability.

Fig. 2 illustrates the schematic diagram of proposed programmable Gaussian-derived Gm-C wavelet filter. The denominator and numerator of (4) and (5) are implemented by Gm cells g_j (j=1, 2, …, n) and g_a independently. As shown in Table 1, switches are programed to generate Gaussian and Marr wavelet transforms by simply moving the input transconductor g_a to ① and ②. Switches S_1 and S_2 ensures the selection of wavelets, while S_3~S_6 are employed to realize the minus sign in (4) by exchanging the two input terminals of transconductor g_a.

TABLE 1
Programmability of Wavelet Filter Realized by Switches

Wavelet	S_1	S_2	S_3	S_4	S_5	S_6
Gaussian	1	0	1	0	0	1
Marr	0	1	0	1	1	0

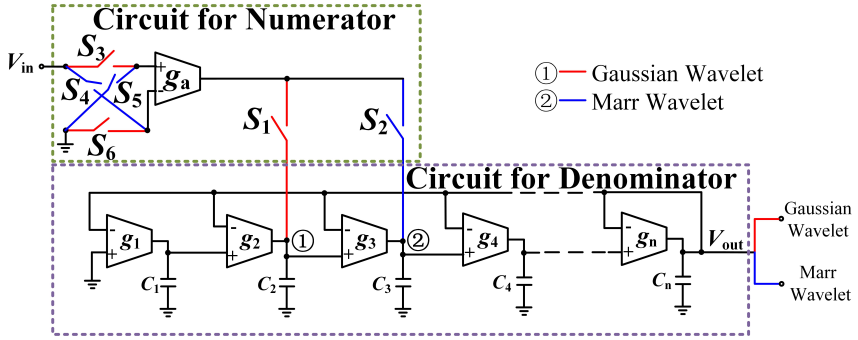

Fig. 2. Schematic diagram of programmable Gaussian-derived Gm-C wavelet filter.

Denoting $\tau_j=C_j/g_j$, the design formula for denominator implementation is given as [16]

$$\tau_n = \frac{B_n}{B_{n-1}}, \tau_{n-1} = \frac{B_{n-1}}{B_{n-2}}, ..., \tau_1 = B_1 \tag{6}$$

Theoretically, the numerator can be realized by zero coefficient β, denoting $\beta=g_a/g_j$. According to [16], each numerator coefficient in transfer function can be realized independently by adding an input transconductor to the corresponding node connected with the capacitor in IFLF structure. As for Fig. 2, the numerator coefficients of (4) and (5) can be generated by connecting g_a with node ① and ②, respectively.

To synthesize (4) and (5), the design formula for β can be expressed as

$$\beta_M = \frac{-A}{B_2}, \quad \beta_G = \frac{A}{B_1} \tag{7}$$

It should be noted that numerator coefficient A in (4) and (5) can be regarded as filter gain. The inaccurate realization of A can be compensated in subsequent stage. Actually, realization deviation of A only introduces changes in absolute amplitude, not the relative amplitude of wavelet transform coefficient which plays an important role in threshold-dependent signal processing. Therefore, the numerator coefficient matching is not considered.

As seen from Fig. 2, the proposed wavelet filter can realize Gaussian and Marr wavelet transforms flexibly by programming switch array with compact structure and minimum components. The same circuit complexity as that of fixed-type wavelet filter can be achieved, which is very suitable for small-size and low-power application.

As a first step, the construction of analog wavelet base as (4) plays an important role in programmable wavelet filter design. Reference [3] provides a valuable method to deduce (4) by using optimization technique, but has relatively low approximation accuracy. To overcome the limitation, this paper presents a novel method to decrease the approximation error between (4) and ideal Marr wavelet, in which the approximation model is constructed and optimized both in time domain.

II. Approximation of Wavelet Base in Time Domain

A. *Mathematical Approximation Model*

Till now, two approximation methods have been proposed to obtain the analog wavelet base shown as (4), which are conducted in frequency domain [3], [17]. Although successful in many aspects, the proposed methods can not yield a high approximation accuracy in time domain. According to Parseval's theorem, making the fitting error of analog wavelet base minimum in time domain can guarantee high approximation accuracy both in time and frequency domain [2]. Therefore, this paper aims to propose a novel method to construct analog Marr wavelet base in time domain with only one numerator term.

Wavelet bases are usually noncausal and cannot be directly implemented by analog filter. Thus, a time delay t_0 should be introduced. Assume $h(t)$ and $\psi_M(t_0-t)$ are the impulse response of analog wavelet base and the time-reversed Marr wavelet delayed by t_0, respectively. Obviously, the optimal approximation in time domain can be found when $h(t)$ and $\psi_M(t_0-t)$ have the same waveform. Hence, the core task for constructing analog wavelet base is to find the minimum fitting error between $h(t)$ and $\psi_M(t_0-t)$ by optimizing coefficients in (4).

Herein, L_2-norm calculated by numerical approach with discretization is used to quantify the fitting error. Also, to evaluate the fitting error in time domain, $h(t)$ is derived from (4) by using Inverse Laplace Transform, i.e.,

$$h(t) = L^{-1}(H_M(s)) \tag{8}$$

where L^{-1} denotes the operator of Inverse Laplace Transform.

To design a stable wavelet filter, the denominator of analog wavelet base should be a strictly Hurwitz polynomial, that is, the denominator of (4) should have positive coefficients and the roots with negative real part. Simultaneously, the selection of time delay t_0 should be balanced delicately. Large t_0 will increase the range close to zero near the origin, which means high-order wavelet filter is required to yield a satisfied approximation result. Small t_0 may introduce large truncation error and deteriorate the overall approximation accuracy. Clearly, improper selection of t_0 may lead to large chip size and high power consumption that are not welcome in wearable sensor design. Unfortunately, in almost all the existing time-domain approximation methods, the value of t_0 is not considered as an important parameter to be optimized, but assigned to a pre-set value manually.

Instead, the denominator coefficients B_i (i=1, 2…n) in (4) and also the time delay t_0 are used in this paper to construct the mathematic model for approximating Marr wavelet base, which can be defined as

$$\min \quad E(B_i,t_0) = \sqrt{\sum_{k=0}^{K}[h(k\Delta T)-\psi_M(t_0-k\Delta T)]^2} \tag{9}$$

$$s.t. \quad B_i > 0,\ real(p_i) < 0,\ i = 1,2,...,n$$

where p_i represents the pole of designed analog wavelet base $H_M(s)$, K+1 is the number of sampling points and ΔT is the sampling interval.

As seen from (9), the approximation of Marr wavelet in time domain essentially is an optimization problem. In this paper, the HAFSA is proposed to find the optimal solution of B_i and t_0.

B. *Hybrid Artificial Fish Swarm Algorithm*

Artificial Fish Swarm Algorithm (AFSA) is an effective technique to deal with optimization problem thanks to the insensitivity to initial value selection and high performance in global search [18]-[22]. However, AFSA has the disadvantage of premature convergence and is easily trapped into local optima. Herein, sequential quadratic programming (SQP) is employed to overcome above limitation. As a local search method, SQP can locate the local optima efficiently, but is sensitive to the selected initial solution. In this context, the hybrid AFSA (HAFSA) consisting of AFSA and SQP is proposed, in which AFSA is used to locate the near-globally optima and provide the initial solution for SQP.

1) *Artificial Fish Swarm Algorithm*

The AFSA is a heuristic optimization method designed by simulating the foraging behavior of fish school. In nature, fishes are willing to stay in the environment with rich nutrient. As the fictitious entity of true fish, artificial fish is used to represent a candidate solution in optimization problem. Generally, AFSA searches the optimum solution by imitating fish swarm behaviors, including prey, swarm, follow and random. Herein, the principle of AFSA is illustrated by taking the maximum problem as an example.

Prey Behavior. As a biological behavior, artificial fish tends to prey at the place with high food concentration. Assume the current state of artificial fish is at X_i. Then, a new state X_j is selected randomly within the perception distance *Visual*, which can be represented by

$$X_j = X_i + Visual \cdot rand(0,1) \tag{10}$$

where *rand*(0,1) generates a random number between 0 and 1. Herein, the food concentration at X_i is represented by $f(X_i)$. If $f(X_j)>f(X_i)$, the artificial fish swims forward a step in this direction. The next state $X_i^{(k+1)}$ of artificial fish can be expressed by

$$X_i^{(k+1)} = X_i^{(k)} + \frac{X_j - X_i^{(k)}}{\| X_j - X_i^{(k)} \|} \cdot Step \cdot rand(0,1) \tag{11}$$

where *Step* is the moving step length.

Otherwise, the new state X_j is selected randomly again based on (10). If the preset number of repeated attempts *Try_num* is exceeded, artificial fish will swim forward a step randomly.

Swarm Behavior. As a natural living habit, fishes usually gather into groups to facilitate forage and avoid predators. Assume the current state of artificial fish is at X_i. In addition, there exist n individual companions within its perception distance *Visual*. X_c is the center position of individual companions. δ is the congestion degree of fish swarm. If $f(X_c)/n>\delta f(X_i)$, it means that the food concentration is high around center position X_c, and the surrounding is not crowded. Then, the artificial fish swims forward a step in the direction of center position. The next state $X_i^{(k+1)}$ of artificial fish can be expressed by

$$X_i^{(k+1)} = X_i^{(k)} + \frac{X_c - X_i^{(k)}}{\| X_c - X_i^{(k)} \|} \cdot Step \cdot rand(0,1) \tag{12}$$

Otherwise, the prey behavior is executed.

Follow Behavior. During the process of foraging, fishes usually follow their companions which have found the food.

Assume X_i is the current state of artificial fish. Then, X_j is the state within perception distance which has the highest food concentration $f(X_j)$. If $f(X_j)/n>\delta f(X_i)$, it means that the surrounding is not crowded around position X_j. The next state $X_i^{(k+1)}$ of artificial fish can be given as

$$X_i^{(k+1)} = X_i^{(k)} + \frac{X_j - X_i^{(k)}}{\| X_j - X_i^{(k)} \|} \cdot Step \cdot rand(0,1) \tag{13}$$

Otherwise, the prey behavior is carried out.

Random Behavior. By imitating the activity of random swim in fish's living habit, random behavior is used to alleviate the premature problem of falling into local optima. The process for random behavior can be described as

$$X_i^{(k+1)} = X_i^{(k)} + Visual \cdot rand(0,1) \tag{14}$$

where $X_i^{(k)}$ and $X_i^{(k+1)}$ are the current state and the new state, respectively.

2) *Sequential Quadratic Programming Algorithm*

Sequential quadratic programming is one of the most powerful tools for nonlinearly constrained optimization problems.

In SQP algorithm, the nonlinear optimization problem is solved by using an iterative procedure. At each iteration x^k, the optimization problem (9) is modeled by a quadratic programming (QP) subproblem, i.e.

$$\min_d \nabla f(x^k)^{\mathrm{T}} d + \frac{1}{2} d^{\mathrm{T}} W(x^k, \lambda^k) d \tag{15}$$

where $f(x_k)$ denotes the objective function E in (9), d is the descent direction and $W(x^k, \lambda^k)$ represents the Hessian of the Lagrangian for problem (9).

Then, a new iteration x^{k+1} is constructed by solving the QP subproblem, i.e.,

$$x^{k+1} = x^k + d \tag{16}$$

Moreover, the constrained condition in problem (9) needs to be dealt with. Herein, the constraint for B_i can be realized simply by setting the lower bound on the optimization variables. Meanwhile, to obtain stable analog wavelet base, a penalty term $rP(x)$ is introduced to the fitness function of artificial fishes when poles are located at the right half of s-plane, in which r denotes the penalty coefficient, $P(x)$ is the penalty function and x represents the feasible solution. In this paper, r and $P(x)$ are constructed by exterior penalty function, defined as

$$\begin{cases} r = (iter/2)^2 \\ P(x) = \max(real(p_i), 0) \end{cases} \tag{17}$$

where *iter* is the number of iterations.

Finally, the mathematical model for approximating Marr wavelet in time domain can be expressed based on (9) and (17), i.e.,

$$\min \quad E(B_i,t_0)=\sqrt{\sum_{k=0}^{K}[h(k\Delta T)-\psi_M(t_0-k\Delta T)]^2} \qquad (18)$$
$$+(iter/2)^2\cdot\max(real(p_i),0),\ i=1,2,\ldots n$$

3) *Implementation Steps for HAFSA*

Taking all the considerations into account, the implementation steps of proposed HAFSA is summarized as below.

Step 1: Set the parameters in AFSA, including maximum number of iterations *Maxiter*, number of artificial fishes *N*, and also *Try_num*, δ, *Step* and *Visual*.

Step 2: Initialize the state of artificial fishes $X^{(1)}$ and set *iter*=1.

Step 3: Perform swarm and follow behaviours simultaneously at the current state of the *i*th artificial fish $X_i^{(k)}$. If $f(X_c)/n>\delta f(X_i^{(k)})$ and $f(X_j)/n>\delta f(X_i)$, the new states $X_i^{(k+1)}$ and $X_i^{(k+1)}$ are determined according to (12) and (13), respectively. And then, jump to Step 5. Otherwise, go to Step 4.

Step 4: Perform prey behavior. The next state of the *i*th artificial fish is obtained according to (11) and then jump to Step 6.

Step 5: Compare food concentration $f(X_i^{(k+1)})$ with $f(X_i^{(k+1)})$, and select the larger one to determine the next state $X_i^{(k+1)}$.

Step 6: $i=i+1$. If $i\le N$, go back to Step 3; otherwise, go to Step 7.

Step 7: $iter=iter+1$. If $iter\le Maxiter$, let $i=1$ and go back to Step 3; otherwise, select the best artificial fish as the initial solution $x^{(0)}$ and go to Step 8.

Step 8: Initial $W^{(0)}$ in (15) and the allowed maximum error ε.

Step 9: If $\|\nabla f(x^k)\|\le\varepsilon$, stop and select x^k as the optimal solution; otherwise, go to Step 10.

Step 10: Convert the optimization problem (9) to QP subproblem based on (15). Then, determine the search direction *d* and the next iteration x^{k+1}.

Step 11: Calculate the Hessian matrix of Lagrange function $W^{(k+1)}$.

Step 12: let $k=k+1$, and go back to Step 9.

III. Construction of Analog Marr Wavelet Base Using HAFSA

The proposed method can be used to approximate Marr wavelet at arbitrary filter orders. In this paper, the seventh-order analog Marr wavelet base at a=1 is selected to elaborate the design procedure.

According to (9), the mathematical approximation model can be given as

$$\min \quad E(B_i,t_0)=\sqrt{\sum_{k=0}^{2000}[h_{sev}(k\Delta T)-\psi_M(t_0-k\Delta T)]^2} \qquad (19)$$
$$+(iter/2)^2\cdot\max(real(p_i),0),\ i=1,2,...,7$$

The HAFSA is used to find the optimal solution of (19). The parameters in HAFSA are set as: *N*=200, *Maxiter*=200, *Try_num*=100, *Visual*=25, δ=27and *Step*=3.

After 200 iterations by AFSA, the obtained optimal solution is selected as the initial solution of SQP algorithm. Finally, the optimal solution of (19) obtained by HAFSA is B_1=4.4833, B_2=6.1443, B_3=7.6027, B_4=4.1921, B_5=2.6708, B_6=0.5942, B_7=0.226, t_0=3.51. Substituting above parameters into (4), the seventh-order analog Marr wavelet base at a=1 can be given as

$$H(s)=\frac{-2.1741s^2}{0.226s^7+0.5942s^6+2.6708s^5+4.1921s^4+7.6027s^3+6.1443s^2+4.4833s+1} \qquad (20)$$

Fig. 3(a) illustrates the impulse response of (20) compared with existing methods. Noted that only the analog wavelet bases with one term in numerator are considered. Obviously, the proposed method can improve the approximation performance of AFSA by introducing SQP, and yield highest approximation accuracy among exiting methods. Table 2 gives the values of approximation error and time delay t_0 obtained or selected in different methods. Clearly, by introducing t_0 as an optimized parameter in approximation model, the proposed method can find the optimal t_0 for the purpose of enhancing approximation result. Fig. 3(b) shows the frequency response of constructed analog wavelet base. It can be seen that the proposed method can also yield a satisfied approximation result in frequency domain.

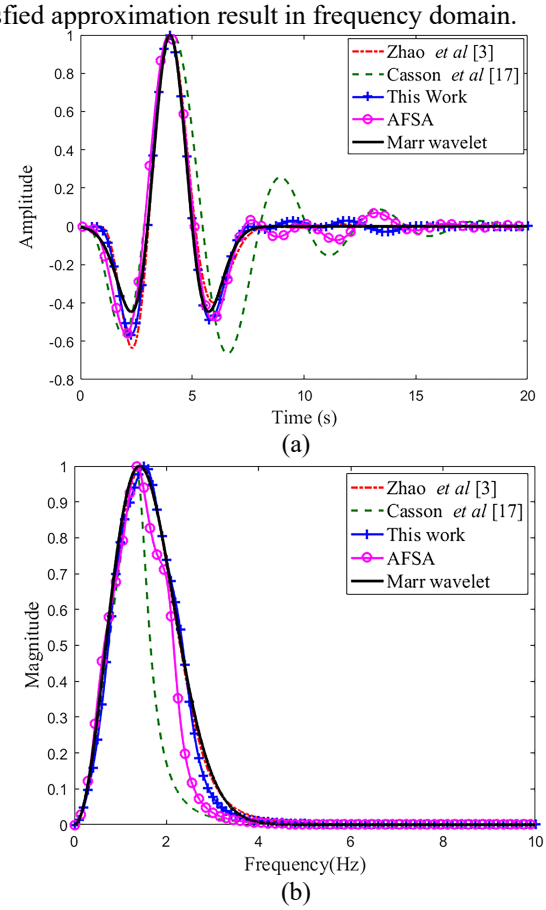

Fig. 3. Approximation of Marr wavelet by proposed method (a) impulse response (b) frequency response.

TABLE 2
COMPARISON OF L_2-NORM APPROXIMATION ERROR IN TIME DOMAIN FOR DIFFERENT APPROXIMATION METHODS.

Spec. \ Method	Casson et al [17]	Zhao et al [3]	AFSA	This work (HAFSA)
Order	7	7	7	7
Approximation error	5.3	2	2.05	1
Time delay t_0	4s	3.3s	3.9s	3.5s

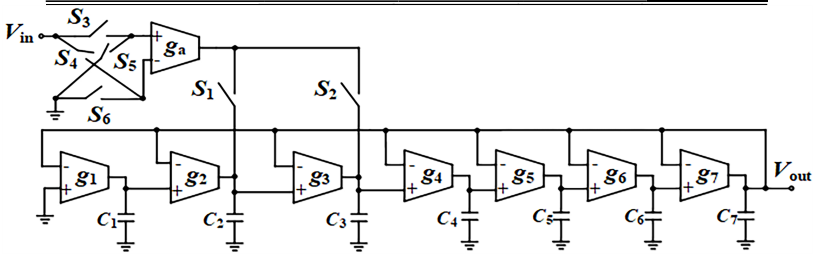

Fig. 4. Seventh-order programmable Gm-C wavelet filter.

$$H(s)=\frac{-0.021741s^2}{2.26\times10^{-8}s^7+5.942\times10^{-7}s^6+2.67\times10^{-5}s^5+4.19\times10^{-4}s^4+7.6\times10^{-3}s^3+6.15\times10^{-2}s^2+0.48s+1} \quad (21)$$

IV. DESIGN OF PROGRAMMABLE GAUSSIAN-DERIVED GM-C WAVELET FILTER

Fig. 4 shows the seventh-order programmable Gaussian-derived Gm-C wavelet filter derived from Fig. 2. Due to the bandpass characteristic in frequency domain, the desired wavelet scales can be realized by denormalizing (20) to related center frequency f_0. Herein, to extract the features of bio-signals commonly in 0-100 Hz range, e.g., ECG and EEG, scale a=0.1 (f_0 =2.5Hz) is chosen as a design example. The transfer function at a=0.1 is written as (21).

To keep the capacitance realistic for chip fabrication in low frequency application, the transconductance of integrator transconductors in Fig. 4 are set to be g_1=100pS, g_2=100pS, g_3=300pS, g_4=200pS, g_5=300pS, g_6=500pS, g_7=500pS. Then, the capacitance values in Fig. 4 can be calculated as C_1=44.833pF, C_2=13.7pF, C_3=37.11pF, C_4=11.02pF, C_5=19.11pF, C_6=11.1pF, C_7=19pF. The transconductance of input transconductor g_a is -106pS calculated by $-A/B_2$ in (21).

To facilitate low voltage and low power operation, the transconductor consisting of simple differential pair is employed [3]. Fig. 5 shows the structure of Gm circuit, with all transistors working in deep weak inversion. The values of transconductance can be realized by setting bias current I_{bias}. For example, g_1=100pS can be obtained by setting I_{bias}=6.5pA.

To provide a low impedance path, all the switches in Fig. 4 are implemented by small size NMOS transistors.

V. SIMULATION RESULTS

The programmable wavelet filter at a=0.1 is designed using standard SMIC 0.18μm, MIM-cap, 1 poly 6 metal CMOS process with 1V power supply.

By programming switches according to Table 1, Gaussian and Marr wavelets can be generated flexibly with minimum circuit components. Fig. 6 and Fig. 7 illustrate the simulated response of generated Gaussian and Marr wavelet filters, respectively. Apparently, the simulated post-layout responses are satisfied compared with ideal wavelet bases and pre-layout simulation results.

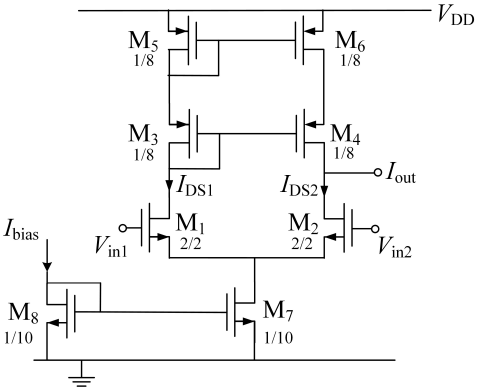

Fig. 5. Circuit structure of Gm cell.

Table 3 summarizes the simulated filter specifications. The signal input range is calculated for a 1% total harmonic distortion (THD). Assume that the input signal of a filter is a sinusoidal signal of fundamental frequency f. Then, the THD can be calculated by [23]

$$\mathrm{THD}=\sqrt{\frac{\sum_{k=2}^{\infty}V_{h_k}^2}{V_f^2}}\cdot100\% \quad (22)$$

where V_f is the amplitude of the fundamental tone, V_{h_k} is the amplitude of the k^{th} harmonic.

In addition, the input reference noise can be obtained by dividing the output noise by the magnitude response, in which the output noise is measured by observing the output frequency spectrum when no input is applied to the filter [24]. The third-order intermodulation distortion (IMD3) of Gaussian wavelet filter can be measured when sine waves at 2 and 2.1Hz are applied. Both input components have same amplitude 5mV giving a 20mVpp input signal [24]. As for Marr wavelet filter, sine waves at 2.5 and 2.6Hz are applied so that the modulation products can fall within the passband of filter [24]. The DR and signal-to-noise ratio (SNR) can be calculated by (23) and (24), respectively.

$$\mathrm{DR}=20\log_{10}^{(\frac{V_{\mathrm{im}}}{V_{\mathrm{floor}}})} \tag{23}$$

$$\mathrm{SNR}=10\log_{10}^{(\frac{V_{\mathrm{irms}}^2}{V_{\mathrm{noise}}^2})} \tag{24}$$

where V_{im} is the maximum input signal voltage, V_{floor} is the noise floor, V_{irms} and V_{noise} represent the input root-mean-square and the input-referred noise voltage, respectively [3].

Also, the figure-of-merit (FoM) is defined as (25) [17],[25]

$$\mathrm{FoM}=\frac{P\cdot V_{dd}}{n\cdot f_c\cdot DR} \tag{25}$$

where P is the filter power consumption, n and f_c represent the number of poles and the center frequency, respectively. Low FoM values are desired for high performance filter design.

To evaluate the effect of process parameters variation and mismatch, a 100 runs Monte Carlo simulation of designed wavelet filter is shown in Fig. 8. As can be seen in Fig 8(a), the frequency responses are close to each other when running a simulation over 100 times using Monte Carlo. In addition, Fig. 8(b) shows that the standard deviation (SD) of the bandwidth at center frequency 5Hz (i.e., scale a=0.05) is only 0.1Hz. Obviously, the designed wavelet filter shows a strong reliability for mismatch and process parameters variation.

The scale of wavelet filter can be adjusted by changing the transconductance value of Gm cells. For example, wavelet scales at 0.1, 0.05, 0.025, 0.0125 and 0.00625 can be implemented by setting bias current I_{bias} of each Gm cell in Fig. 4, which is shown in Table 4. Fig. 9 shows the frequency responses of Marr wavelet filter at different wavelet scales. Apparently, the proposed design method can realize the wavelet transform coefficients at different scales accurately.

Owing to the programmable structure, the proposed method can implement two wavelet bases using minimum circuit complexity and thus lowest power consumption. At scale a=0.1, the center frequency of 2 Hz for Gaussian wavelet and 2.5 Hz for Marr wavelet are achieved with ultra-low power consumption of 141pW.

Fig. 10 shows the performance of proposed wavelet filter in feature extraction of physiological signals, namely wavelet coefficients. The generated Gaussian wavelet filter is used to extracting features from ECG, while Marr wavelet filter is for feature extraction of EEG. The proposed wavelet filter can achieve almost the same performance in feature extraction as analog wavelet bases, which is very suitable for biomedical signal processing in low power and small size application.

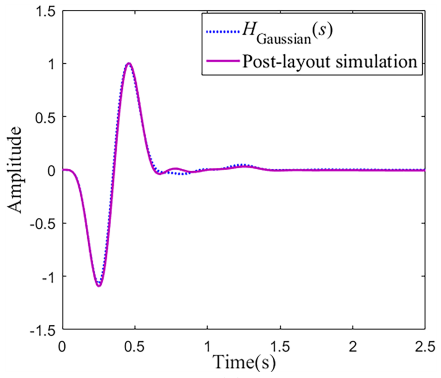

(a)

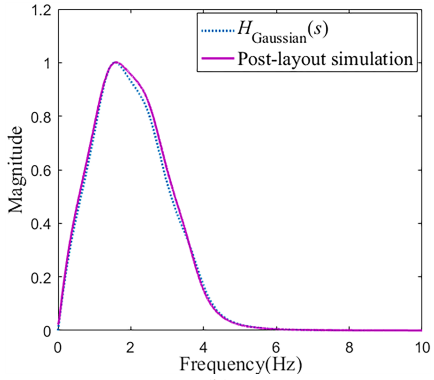

(b)

Fig. 6. Simulated response of Gaussian wavelet filter (a) Impulse response (b) Frequency response.

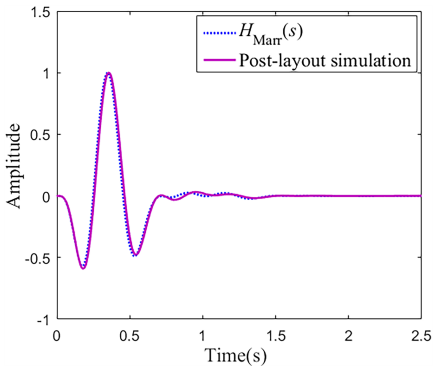

(a)

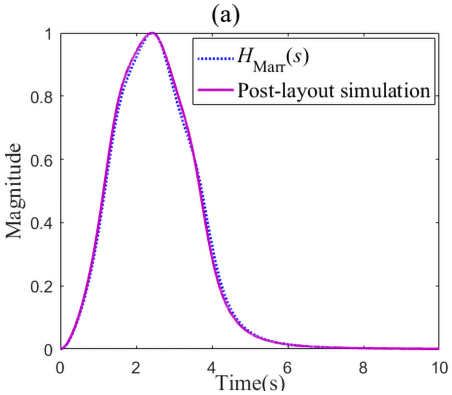

(b)

Fig. 7. Simulated response of Marr wavelet filter (a) Impulse response (b) Frequency response.

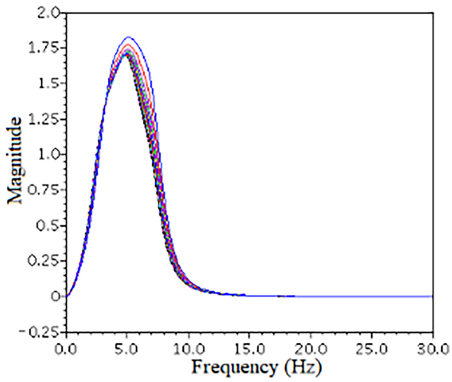

(a)

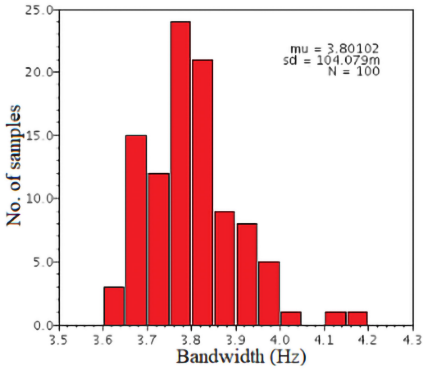

(b)

Figure 8. (a) A 100 runs Monte Carlo simulation of frequency responseof designed wavelet filter at f_c=5Hz (b) mismatch and process parameters variation on the bandwidth for the designed wavelet filter at f_c=5Hz.

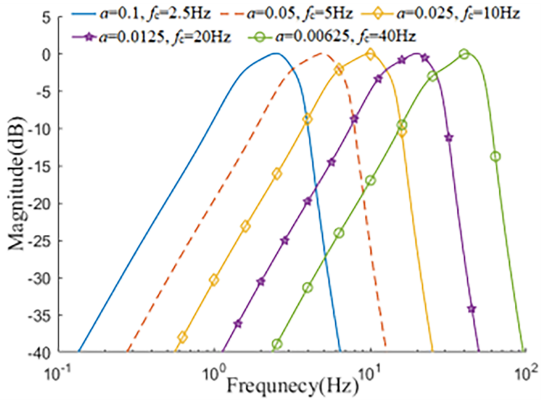

Figure 9. Simulated response of designed Marr wavelet filter at different scales.

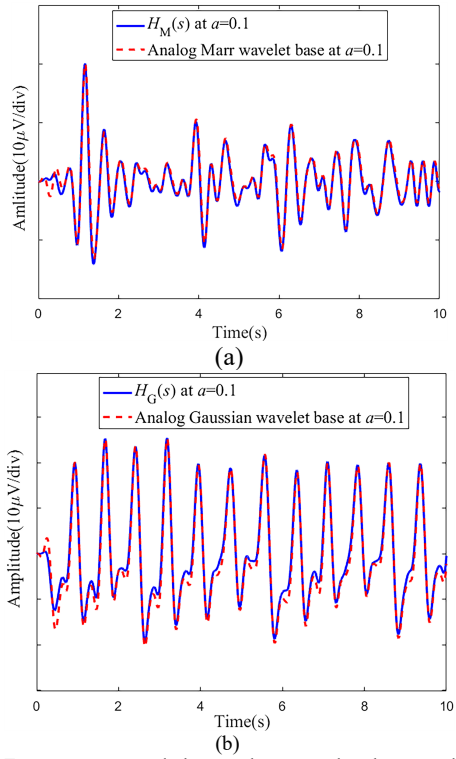

Figure 10. Features extracted by analog wavelet base and designed programmable wavelet filter (a) EEG feature extracted by Marr wavelet (b) ECG feature extracted by Gaussian wavelet.

TABLE 3
SUMMARY OF WAVELET FILTER'S PERFORMANCE.

Spec. \ Wavelet	Gaussian		Marr	
	Pre-layout	Post-layout	Pre-layout	Post-layout
Power (pW)	138	141.68	138	141.68
Signal input range (mVpp)	20	20	20	20
DR (dB)	42.1	42.6	39	39.5
SNR (dB)	39.1	40	33	33.5
Input reference noise (μVrms)	78.3	74.2	158	149
IMD3 (dBc)	-32	-32	-45	-44
THD	1%	1%	1%	1%
FoM (10^{-13})	2.34	2.4	2.02	2.05

TABLE 4
BIAS CURRENT VALUE OF EACH TRANSCONDUCTOR IN FIG.4 FOR REALIZING FIVE CENTER FREQUENCIES

Gm	I_{bias}/pA				
	f_c=2.5Hz	f_c=5Hz	f_c=10Hz	f_c=20Hz	f_c=40Hz
g_1	6.3	12.6	25.2	50.4	100.8
g_2	6.3	12.6	25.2	50.4	100.8
g_3	18.9	37.8	75.6	151.2	302.4
g_4	12.6	25.2	50.4	100.8	201.6
g_5	18.9	37.8	75.6	151.2	302.4
g_6	31.5	63	126	252	504
g_7	31.5	63	126	252	504
g_a	4.1	8.1	16	31	56

VI. CONCLUSION

A programmable wavelet filter is proposed for generating multiple-type wavelets. Based on Laplace Transform, the Gaussian and Marr wavelet filters can be realized by moving input transconductor to related internal node with all component parameters unchanged. Then, minimum components are required for filter design, a feature that is very suitable for power-constrained wearable biomedical sensor integrated with local intelligence algorithms. Also, a novel approximation method is presented to construct the analog wavelet base with one numerator term required by programmable characteristic. To enhance the approximation accuracy, the approximation of wavelet base is modeled as an optimization problem in time domain and the HAFSA is proposed to locate the optimal solution.

A seventh-order programmable wavelet filter is designed in 0.18 μm CMOS process. Simulation results demonstrate that an ultra-low power dissipation can be achieved with only 141.68 pW at scale a=0.1. Very low FoM values of 2.4×10^{-13} and $2.05\times10^{-13}$are obtained when generating Gaussian and Marr wavelets, respectively. Experiment result shows that the proposed programmable Gaussian-derived wavelet filter can be

used for accurate extraction of transient features in biomedical signal processing.

VII Data Availability Statement

The data that support the findings of this study are available from the corresponding author upon reasonable request.

REFERENCES

[1] S. Iranmanesh, E. Rodriguez-Villega, "A 950 nW Analog-Based Data Reduction Chip for Wearable EEG Systems in Epilepsy," *IEEE J. Solid-State Circuits*, vol. 52, no. 9, pp. 2362-2373, 2017.

[2] J.M.H. Karel, S.A.P. Haddad, S. Hiseni, *et al*., "Implementing Wavelets in Continuous-Time Analog Circuits With Dynamic Range Optimization," *IEEE Trans. Circuits Syst.*, vol. 59, no. 2, pp. 229-242, 2012.

[3] W. Zhao, L. Ma, Y. Zhang, *et al*., "Realization of Analog Wavelet Filter Using Hybrid Genetic Algorithm for On-Line Epileptic Event Detection," *IEEE Access*, vol. 8, pp. 33137-33150, 2020.

[4] M. Li, and Y. Sun, "General rational approximation of Gaussian wavelet series and continuous-time gm-C filter implementation," *Int J Circ Theor App.*,vol. 48, pp. 2006-2022, 2020.

[5] G. Makkena, P. R. BVVSN and M. B. Srinivas, "Uniform approximation of Gaussian wavelet for biomedical signal processing in analog domain," *2013 35th Annual International Conference of the IEEE Engineering in Medicine and Biology Society* (EMBC), Osaka, Japan, pp. 2886-2889, 2013.

[6] W. Zhao, L. Ma, Y. Zhang, *et al.*, "Design of Gm-C wavelet filter for on-line epileptic EEG detection," *IEICE Electronics Express*, vol 16, no. 23, 2019.

[7] X. Xie et al., "An ECG feature extraction with wavelet algorithm for personal healthcare," *2015 International Symposium on Bioelectronics and Bioinformatics* (ISBB), Beijing, China, pp. 128-131, 2015.

[8] A. J. Casson, E. Rodriguez-Villegas, "Nanowatt multi-scale continuous wavelet transform chip," *Electronics Letters*, vol. 50, no. 3, pp. 153-154, 2014.

[9] J. Rafiee, M.A. Rafiee, N. Prause, *et al*., "Wavelet basis functions in biomedical signal processing," *Expert Systems with Applications*, vol. 38, no. 5, pp. 6190-6201, 2011.

[10] H. He, Y. Tan and Y. Wang, "Optimal Base Wavelet Selection for ECG Noise Reduction Using a Comprehensive Entropy Criterion," *Entropy*, pp. Vol. 17, no. 9, 6093-6109, 2015.

[11] L. Stanke, J. Kubiek, D. Vilimek, *et al*., "Towards to Optimal Wavelet Denoising Scheme-A Novel Spatial and Volumetric Mapping of Wavelet-Based Biomedical Data Smoothing," *Sensors*, vol. 20, no. 18, 2020.

[12] I. Mporas, V. Tsirka, E. I. Zacharaki, *et al*., "Seizure detection using EEG and ECG signals for computer-based monitoring, analysis and management of epileptic patients," *Expert Systems with Applications*, vol. 42, no. 6, pp. 3227-3233, 2015.

[13] A. Shoeb, T. Pang, J. Guttag, S. Schachter, "Non-invasive computerized system for automatically initiating vagus nerve stimulation following patient-specific detection of seizures or epileptiform discharges," *Int J Neural Syst*, vol. 19, no. 3, pp. 157-172, 2009.

[14] I. Mporas , V. Tsirka, E.I. Zacharaki, *et al.*, "Online Seizure Detection from EEG and ECG Signals for Monitoring of Epileptic Patients," *Hellenic Conference on Artificial Intelligence. Springer*, Cham, pp. 442-447, 2014.

[15] Y. Liu, S. Sivathamboo, P. Goodin, *et al*., "Epileptic Seizure Detection Using Convolutional Neural Network: A Multi-Biosignal study," *Proceedings of the Australasian Computer Science Week Multiconference*, New York, NY, USA, 2020.

[16] W. Zhao, Y. Sun, Y. He, "Minimum component high frequency Gm-C wavelet filters based on Maclaurin series and multiple loop feedback," *Electron. Lett.*, vol. 46, no. 1, pp. 34-36, 2010.

[17] A. J. Casson, E. Rodriguez-Villegas, "A 60pW gmC Continuous Wavelet Transform Circuit for Portable EEG Systems," *IEEE Journal of Solid-State Circuits*, vol. 46, no. 6, pp. 1406-1415, 2011.

[18] Y. Hu, K. Lv, "Hybrid Prediction Model for the Interindustry Carbon Emissions Transfer Network Based on the Grey Model and General Vector Machine," *IEEE Access*, vol. 8, pp. 20616-20627, 2020.

[19] X. Zhou, X. Yu, Y. Zhang, Y. Luo and X. Peng, "Trajectory Planning and Tracking Strategy Applied to an Unmanned Ground Vehicle in the Presence of Obstacles," *IEEE Transactions on Automation Science and Engineering*, pp. 1-15, 2020.

[20] X. Zhou, Z. Wang, D. Li, H. Zhou, Y. Qin and J. Wang, "Guidance Systematic Error Separation for Mobile Launch Vehicles Using Artificial Fish Swarm Algorithm," in IEEE Access, vol. 7, pp. 31422-31434, 2019.

[21] Y. QI, P. ZHI, H. YE and W. ZHU, "Research on Lifetime Optimization of Unmanned Ship Lithium Battery Pack Power Supply System Based on Artificial Fish Swarm Algorithm," *2020 39th Chinese Control Conference* (CCC), Shenyang, China, pp. 5379-5384, 2020.

[22] W. Yao, B. Yi, T. Huang and W. Li, "Poisson Robust Soliton Distribution for LT Codes," *IEEE Communications Letters*, vol. 20, no. 8, pp. 1499-1502, 2016.

[23] D. Baxevanakis and P. P. Sotiriadis, "A General Time-Domain Method for Harmonic Distortion Estimation in CMOS Circuits" *IEEE Transactions on Computer-Aided Design of Integrated Circuits and Systems*, vol. 40, no. 1, pp. 157-170, 2021.

[24] A. J. Casson, "A data reduction algorithm incorporating a low power continuous wavelet transform for use in wearable electroencephalography systems," Ph.D. dissertation, Imperial College of Science, Technology and Medicine Department of Electrical and Electronic Engineering, Imperial College, UK, 2010.

[25] Rao G., H, P., S, S., R, Bhat, MS. A 0.3-V, 2.4-nW, and 100-Hz fourth-order LPF for ECG signal processing. *Int J Circ Theor App.* 48, 2020, 1853-1863